ARTICLE OPEN

Check for updates

The corrosion behavior of EW75 magnesium alloy in the research vessel *KEXUE* during the ocean voyage

Quantong Jiang[1,2,3,4]✉, Dongzhu Lu[1,4], Liren Cheng[2], Nazhen Liu[1,4], Lihui Yang[1,4] and Baorong Hou[1,3,4]

The corrosion behavior of EW75 magnesium alloy in the Research Vessel *KEXUE* (*RV KEXUE*) during the ocean voyage was researched. The weight loss, corrosion depths, corrosion morphologies, and corrosion products were all analyzed. The mean weight loss rate of EW75 alloy Extrusion Surface was 0.0672 mg cm^{-2} y^{-1} (0.0903 mm y^{-1}) after exposure corrosion tests, whereas that of Cross-section Surface was 0.0938 mg cm^{-2} y^{-1} (0.1537 mm y^{-1}). Both extrusion direction and transverse direction of magnesium alloy samples occurred the brittle fracture in the harsh marine environment, and the mechanical strength fell precipitously after the exposure tests. The corrosion resistance of EW75 magnesium alloys obviously showed the anisotropy, which was due to the texture of the magnesium alloy in the microstructure. High salinity and high humidity environment led to a severe corrosion of EW75 magnesium alloys during exposure in the *RV KEXUE* during the ocean voyage. This study will provide the effective data for the service of magnesium alloys in typical marine atmospheric environment.

npj Materials Degradation (2022)6:28; https://doi.org/10.1038/s41529-022-00238-0

INTRODUCTION

Magnesium alloys are the lightest structural metallic materials, which are widely used in aerospace, military and other fields[1,2]. With the implementation of the marine power strategy in the world, the marine atmospheric environment has become one of the important service environments for advanced magnesium alloy materials and their structural parts. Carrier rockets have started to launch from the sea in order to meet the needs of low-inclination orbit satellite launch, which require the better corrosion resistance of magnesium alloys in harsh marine corrosive environment. The high-strength magnesium alloys contained rare earths (Mg-RE alloys) have more excellent performance[3,4], which can meet the use requirements of advanced light metal structural parts in the marine atmospheric environment with high salt and high humidity[5,6]. Especially, the Mg-7Gd-5Y-1Nd-0.5Zr (EW75) magnesium alloys have been used in multiple important equipment due to their high mechanical properties at room and elevated temperatures[7–9]. Therefore, research on the corrosion resistance of Mg-RE alloys in typical marine atmospheric environment become the key issue for their application. Corrosion dynamics pattern, residual mechanical strength and failure mechanism of Mg-RE alloys are all need to obtain from the experiments[10–12]. They are used to evaluate the service life of magnesium alloy scientifically in typical marine atmospheric environment.

Liao et al.[13] investigated the marine atmospheric corrosion behavior of AZ31B Mg alloys exposure for 1 year in Shimizu City of Japan, and they obtained that the weight loss rate of FG-AZ31B and CG-AZ31B was about 32.6 and 34.6 μm/y, respectively. Liao et al.[14] also analyzed the corrosion products of AZ31 alloys, and the conclusion showed that $(Mg_{0.833}Al_{0.167})(OH)_2(CO_3)_{0.083}{\cdot}0.75H_2O$ formed on surface of samples during the early exposure period, whereas the corrosion products were mainly consisted of aluminum element after long-term exposure. Martin et al.[15] researched marine atmospheric corrosion of AZ91D alloy from the Atlantic shore in Brest, France and found that the corrosion rate of was 4.2 μm/year. The main corrosion product on AZ91D alloy surface was $(Mg_5(CO_3)_4(OH)_2{\cdot}4H_2O)$. The corrosion attacked originally from the inside of larger α-phase. Cui et al.[16] studied marine atmospheric corrosion behavior of AZ31 alloys in Xisha Islands and analyzed the effect of Cl^- on the corrosion process. They proved that the corrosion crack initiated from pit etching and then extended to general corrosion, while the main corrosion product was $Mg_5(CO_3)_4(OH)_2{\cdot}xH_2O$. Cui et al.[17] also researched pitting corrosion behavior of AZ31 alloy in Xisha Islands and found that pit etching was the primary corrosion form. The corrosion process was consisted of initiation and propagation of corrosion pit etching. Liu et al.[18] summarized atmospheric corrosion of magnesium alloys in the surface aqueous layer. The main influence factors were contained grains, kinds and distribution of precipitated phases, condition of corrosion products, Cl^-, relative humidity and temperature in the corrosion environment. Jiang et al.[19] researched the corrosion behavior of Mg-Nd alloys in the harsh South China Sea environment and obtained the corrosion rate of Mg-xNd ($x = 0.5$, 1.0, 1.5 wt%) alloy was 0.0837 mm y^{-1}, 0.0693 mm y^{-1} and 0.0517 mm y^{-1}, respectively. The mechanical strength of Mg-Nd binary alloy was damaged severely due to the heavy rainfall and high humidity, sodium chloride in South China Sea environment. Jiang et al.[20] also studied the marine atmospheric corrosion pattern of Mg-7Gd-5Y-1Nd-0.5Zr alloys at Qingdao site, and they found that the mean corrosion rate was 5.2722 g m^{-2} per month. Relative humidity and inorganic salts were the main influence factors for corrosion process. However, in many cases, structure and equipment in service are in the mobile condition for a long time. That means the practical locations of magnesium alloys materials are not permanent, such as vessel and maritime aircraft. Until now, there are few researches on corrosion experiment of magnesium alloys on the sailing vessel in the typical marine atmospheric environment.

[1]CAS Key Laboratory of Marine Environmental Corrosion and Bio-fouling, Institute of Oceanology, Chinese Academy of Sciences, No. 7 Nanhai Road, 266071 Qingdao, China. [2]State Key laboratory of Rare Earth Resource Utilization, Changchun Institute of Applied Chemistry, Chinese Academy of Sciences, No. 5625 Renmin Street, 130022 Changchun, China. [3]Sanya Institute of Oceanology, South China Sea Institute of Oceanology, Chinese Academy of Sciences, Zhenzhou Road, 572000 Sanya, China. [4]Open Studio for Marine Corrosion and Protection, Pilot National Laboratory for Marine Science and Technology (Qingdao), No.1 Wenhai Road, 266235 Qingdao, China.
✉email: jiangquantong@qdio.ac.cn

In this work, the EW75 magnesium alloys officially served in the military field were picked up as the basic experimental materials, and their exposure corrosion behavior in the *RV KEXUE* during the ocean voyage was researched. The weight loss, corrosion depths, corrosion morphologies and corrosion products were all analyzed. The synergistic effect of the marine environmental factors and anisotropic microstructure on the corrosion behavior of EW75 magnesium alloys was described and discussed. This study will provide the effective data for the service of magnesium alloys in typical marine atmospheric environment.

RESULTS AND DISCUSSION

Microstructure of EW75 magnesium alloys

As shown in Fig. 1, the grain size of EW75 magnesium alloys was small and uniform for both Extrusion Surface and Cross-section Surface. The precipitated phases evenly distributed after deformation and aging. The Extrusion Surface showed the extrusion flow obviously, and precipitated phases distributed along the extrusion direction. On the other hand, the precipitated phases in the Cross-section Surface distributed more diffuse. Previous studies had shown that the precipitated phases of EW75 magnesium alloys were mainly consisted of elliptic spherical β′ phases. The crystal microstructure of precipitated β′phases was base-centered orthorhombic lattice, which lattice parameter was a = 0.64 nm, b = 2.22 nm, c = 0.52 nm, respectively. The structural characteristics model of elliptic spherical β′ phases was Mg_7RE[21–23]. In the EW75 magnesium alloys, the precipitated phases impeded dislocation slip at the room temperature, result that the deformation resistance increased. Consequently, the mechanical strength of EW75 magnesium alloys can reach to more than 450 MPa. As shown in Fig. 1c, d, the average grain size of both the Extrusion Surface samples and Cross-section Surface samples was about 10–20 μm. The grain colors in the maps corresponded to the crystallographic axes shown in the inserted stereographic triangle. We determined that the (0 0 0 1) base planes of most grains were parallel to the ED. The average grain size of the two types of EW75 Magnesium Alloy samples was similar, which implied that the grain-size difference was not responsible for the corrosion-rate difference among the different samples types. Meanwhile, the amount and distribution of precipitated phases on the surface of the two different samples were also basically the same. Therefore, the key factor that determined the difference of corrosion resistance of Extrusion Surface samples and Cross-section Surface samples was that different crystallographic preferred orientations.

The crystallographic texture Extrusion Surface and Cross-section Surface samples were characterized by EBSD. As shown in Fig. 2, different colors represented different orientations of the crystal surfaces. The Extrusion Surface along the direction of extrusion deformation, the main grain orientation was (0 0 0 1) base surface[24]. This phenomenon was because that the C axis of close-packed hexagonal (HCP) crystal structure was parallel to the normal direction during the deformation of the EW75 magnesium alloys. The Cross-section Surface were mainly composed of (1 0−1 0) and (2 −1 −1 0) crystal surfaces. Different energy levels of heterogeneous crystal surfaces, resulted to the huge distinction on electrochemical stability and corrosion resistance[25]. Previous studies had shown that the corrosion rate of different crystallographic planes of magnesium alloys was estimated based on an

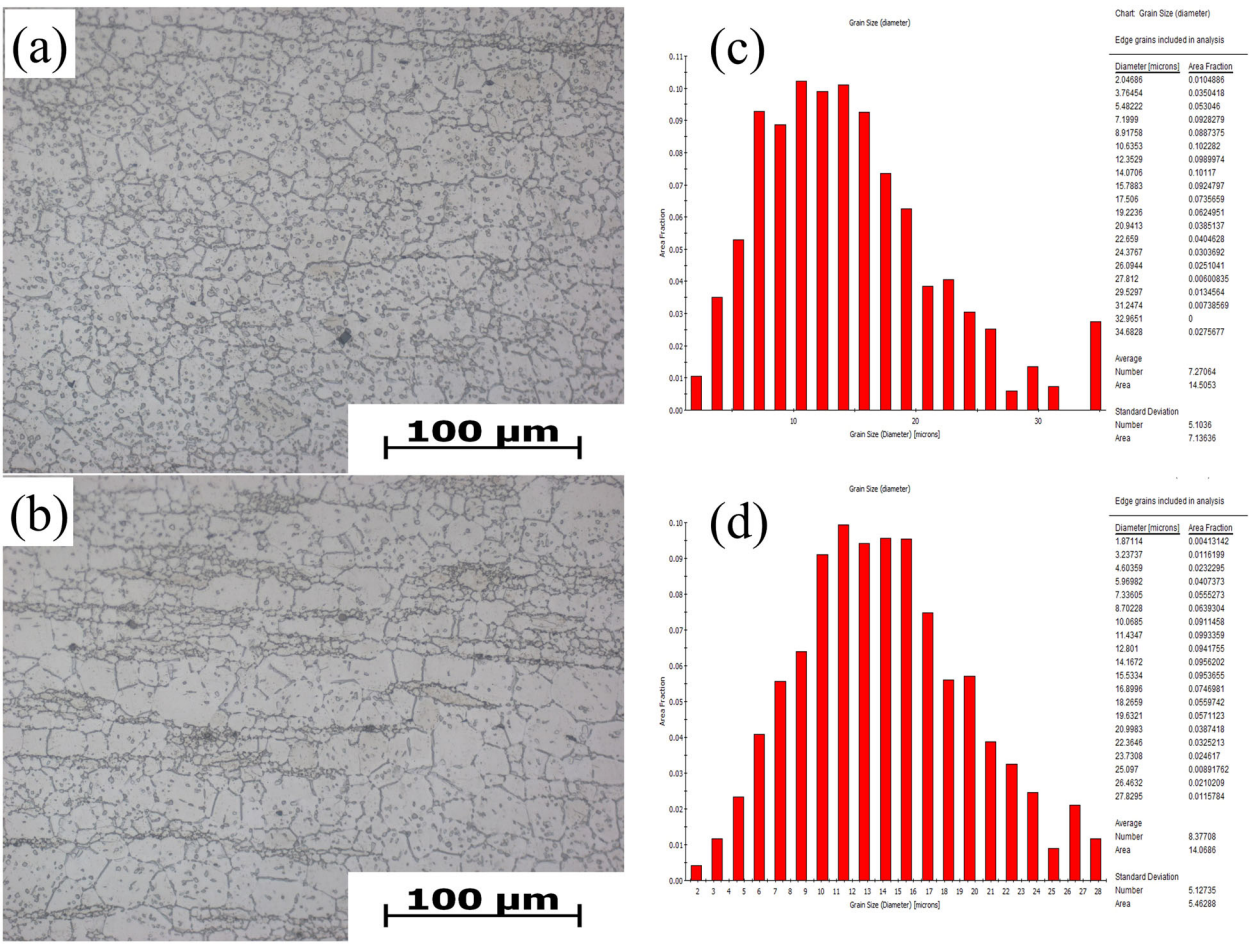

Fig. 1 Microstructureand grain size of different surfaces. a, c Extrusion surface; **b, d** cross-sectionsurface.

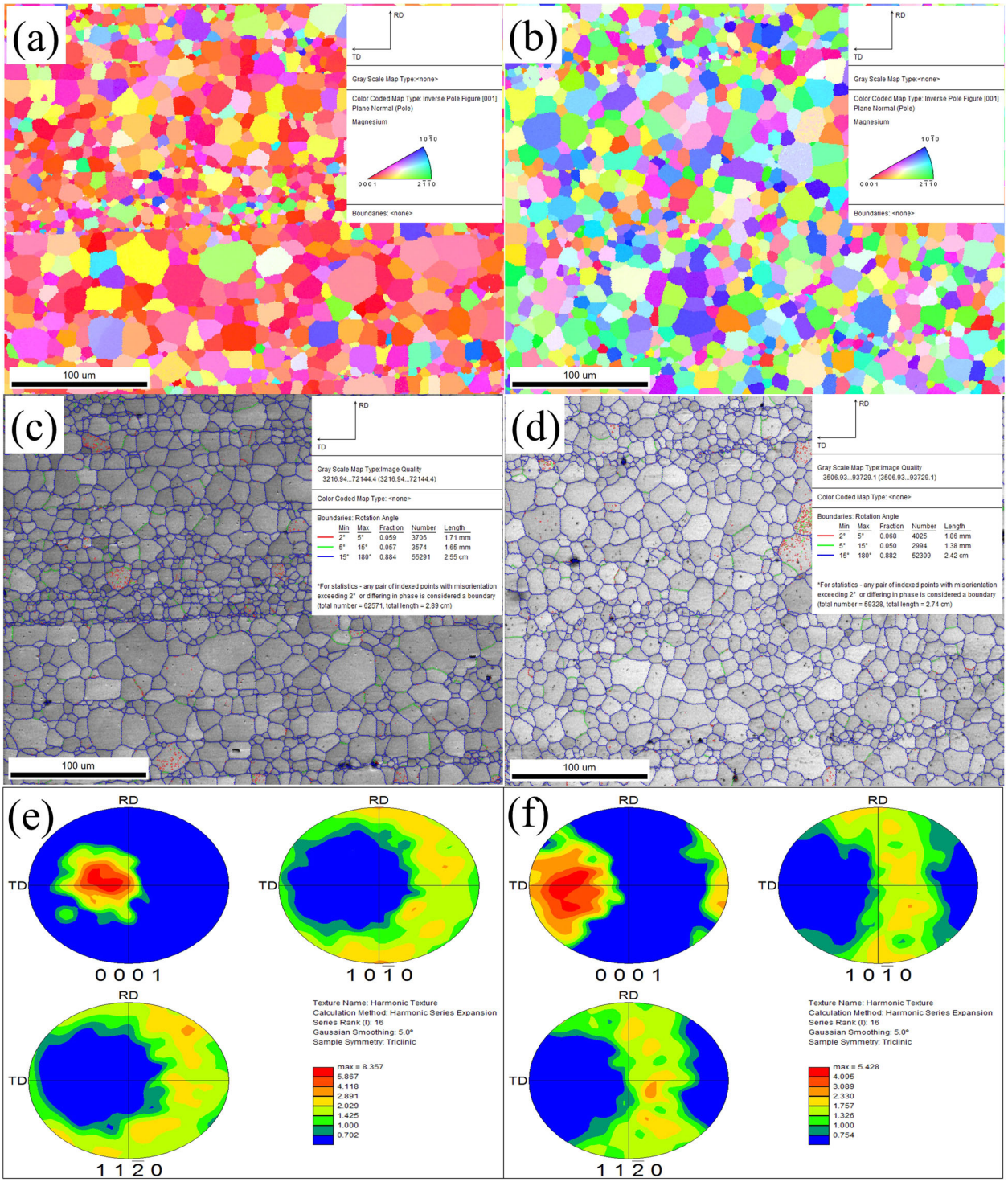

Fig. 2 EBSD analysis of different surfaces. a, **c**, **e** Extrusion surface; **b**, **d**, **f** Cross-section surface.

electrochemical-dissolution-rate equation, and the theoretical dissolution rates of crystallographic planes were as follows: (0 0 0 1) < (1 0 −1 0) < (2 −1 −1 0)[26,27]. The maximum polar density represented the texture intensity of the Extrusion Surface samples and Cross-section Surface samples of EW75 magnesium alloy. This value of Extrusion Surface samples was 8.357, whereas the Cross-section Surface samples was 5.428. The maximum polar density was small, indicated that orientation of the crystal faces was uniform. In this case, relatively uniform corrosion occurred on the surface of magnesium alloys. On the contrary, severe pitting corrosion and location corrosion would occur on the surface of magnesium alloys. Generally, the corrosion resistance of magnesium alloy with relatively uniform corrosion is better.

Surface morphologies and weight loss rate

In this study, ΔW is marked as the value of the weight loss rate of EW75 alloys after more than 3 months exposed corrsion, which unit of measurement is equalled to $g\,cm^{-2}\,y^{-1}$. ΔW can be calculated by the expression: $\Delta W = (W_0 - W_1)/ST$. In this

Table 1. The weight loss rate of EW75 magnesium alloys after 3 months exposed corrsion.

EW75 alloys	Parallel samples	W_0/g	W_1/g	Δ/g	S/cm^2	T/M	ΔW/g cm^{-2} y^{-1}	Average g cm^{-2} y^{-1}
Extrusion Surface	Sample 1	13.5131	12.8798	0.6333	60	3	0.0633	0.0672
	Sample 2	13.4547	12.7760	0.6787	60	3	0.0679	
	Sample 3	13.7167	13.0126	0.7041	60	3	0.0704	
Cross-Section Surface	Sample 1	13.5388	12.5936	0.9452	60	3	0.0945	0.0938
	Sample 2	13.4922	12.5301	0.9621	60	3	0.0962	
	Sample 3	13.5066	12.6013	0.9053	60	3	0.0905	

Table 2. The corrosion depth of EW75 magnesium alloys after 3 months exposed corrsion.

EW75 alloys	Parallel samples	Locations/mm					Average/mm	T /M	Corrosion depth/mm y^{-1}	Average/mm y^{-1}
		①	②	③	④	⑤				
Extrusion Surface	Sample 1	0.0152	0.0147	0.0132	0.0131	0.0143	0.0141	3	0.0846	0.0903
	Sample 2	0.0120	0.0134	0.0168	0.0174	0.0160	0.0151	3	0.0907	
	Sample 3	0.0151	0.016.4	0.0196	0.0166	0.0120	0.0159	3	0.0956	
Cross-Section Surface	Sample 1	0.0285	0.0283	0.0244	0.0210	0.0221	0.0240	3	0.1437	0.1537
	Sample 2	0.0293	0.0258	0.0272	0.0281	0.0281	0.0277	3	0.1662	
	Sample 3	0.0296	0.0242	0.0291	0.0218	0.0214	0.0252	3	0.1513	

expression, W_0 (g) and W_1 (g) means the original weight and the final weight, respectively. W_0 of the EW75 alloys was measured before the exposed corrsion, whereas the W_1 was measured after all the corrosion products were removed from the surface of the alloys. S (cm^2) is equalled to the sum of the six surface areas of each sample. T (y) is behalf of the period of exposed corrsion, which is equalled to 3 months. Actually, the weight loss rate in this study is an average value on the total surface areas of each sample after exposed corrsion. The results were shown in Table 1.

As shown in Table 1, the Extrusion Surface samples had the lowest average corrosion rate 0.0672 g cm^{-2} y^{-1}, whereas the Cross-section Surface samples showed the larger corrosion rate 0.0938 g cm^{-2} y^{-1}. This phenomenon may be attributed to the crystal orientation of texture and distribution of the precipitated phases in the microstructure of Extrusion Surface samples. In fact, the Extrusion Surface of EW75 alloys samples mainly consisting of closely packed crystallographic plane (0 0 0 1) has lower surface energy and thus its anodic dissolution and cathodic hydrogen evolution are more difficult than a Cross-section Surface on which most grains are (1 0 −1 0) and (1 1 −2 0) orientated. As a result, the rolling surface is more corrosion resistant than a Cross-section Surface in marine atmospheric environment. In the present study, the order of weight loss rate is as follows: Extrusion Surface samples < Cross-section Surface.

In addition, the corrosion depth P_W (mm y^{-1}) of EW75 magnesium alloys samples after more than 3 months exposed corrsion was measured via the thickness gauge, and the results were shown in Table 2, as follows. The corrosion depth of Extrusion Surface sample showed a minimum value at 0.0903 mm y^{-1}, whereas that of Cross-section Surface samples showed a maximum value at 0.1537 mm y^{-1}. This phenomemon was also due to the crystal orientation of different surface.

As shown in Fig. 3, the corrosion morphology of EW75 Extrusion Surface and Cross-section Surface samples covered with corrosion products in the *KEXUE* vessel was characterized by optical camera. The metallic luster on the surface of EW75 alloy samples was disappeared, and the surfaces were gradually covered by a layer of white crystalline corrosion products after exposure more than 3 months in the *KEXUE* vessel. Small amounts of brown corrosion product particles existed on the surfaces, this phenomenon might be due to contamination of corrosion products with impurities after washing by seawater and rain. The differences on the surface corrosion morphologies of EW75 Extrusion Surface and Cross-section Surface samples were also apparent to the eyes. The "pitting point" of the white corrosion products on the Extrusion Surface samples had an obvious trend along the direction of the extrusion streamline, whereas the distribution of corrosion products on the Cross-section Surface was relatively uniform. This situation was also determined by the microstructure and texture preference orientation of the EW75 alloys[28].

In typical Marine atmospheric exposure experiment, the corrosion factors of environment and density of corrosion products determined the protective effect on the matrix on on the magnesium alloys[29]. The corrosion products of different EW75 alloy samples were analyzed by XRD after more than 3 months exposure experiment in the *KEXUE* vessel in Fig. 4. As shown in the Fig. 4, the diffraction peaks of magnesium matrix were the largest because that the X-ray reached the matrix through the corrosion product layers. Meanwhile, the diffraction peaks of both (0 0 1) and (1 0 1) crystal surfaces in $Mg(OH)_2$ were very evidently detected in the corrosion products for all the samples. The diffraction peak (0 2 1) crystal surface of $MgCl_2$ in the corrosion products was also detected by the x-ray diffraction. Under normal circumstances, the solubility of $MgCl_2$ was large in the seawater and rain solution, resulted that the residual volume of $MgCl_2$ in the corrosion products was very little. And the diffraction peak of $MgCl_2$ was difficult to be detected in x-ray diffraction analysis. However, in the marine atmospheric environment, the average Cl^- concentration was very high, which led to a serious corrosion of EW75 magnesium alloys. The corrosion product $MgCl_2$ formed a great of quantities on the magnesium matrix surface, so their diffraction peak was also obvious.

When EW75 magnesium alloys exposed to corrode in marine atmospheric environment, the grain boundaries corroded originally due to their high chemical activity. With the gradual corrosion reaction, the $Mg(OH)_2$ corrosion product layers formatted more and more, which improved the layers resistance of grain boundaries and corrosion potential[30]. As the grain boundary potential raised to higher than magnesium matrix, corrosion started to occur inside of the grain. Film formation is highly

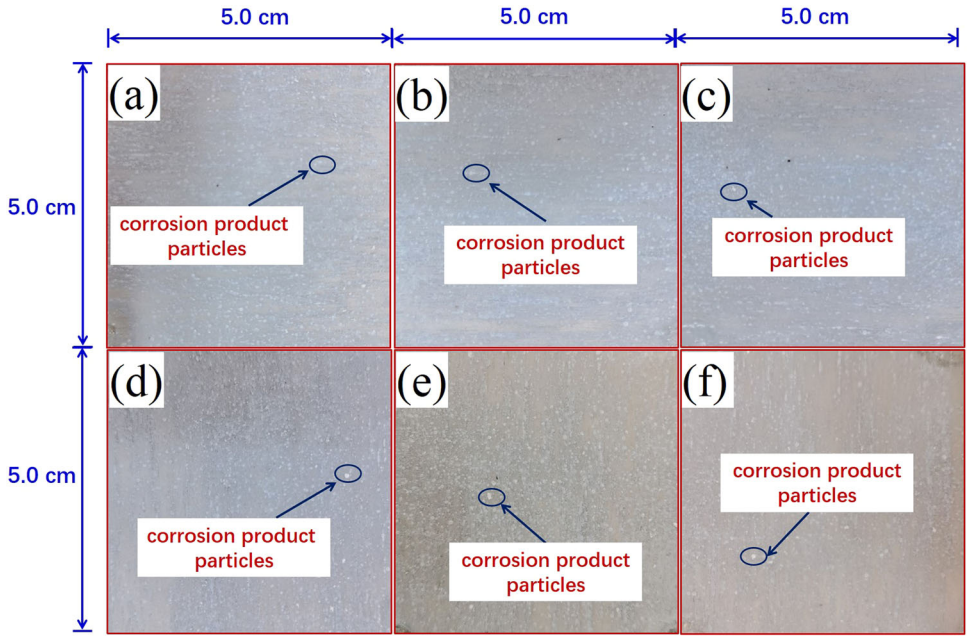

Fig. 3 Corrosion morphologies with corrosion products. a–c Extrusion samples; **d–f** Cross-section surface samples.

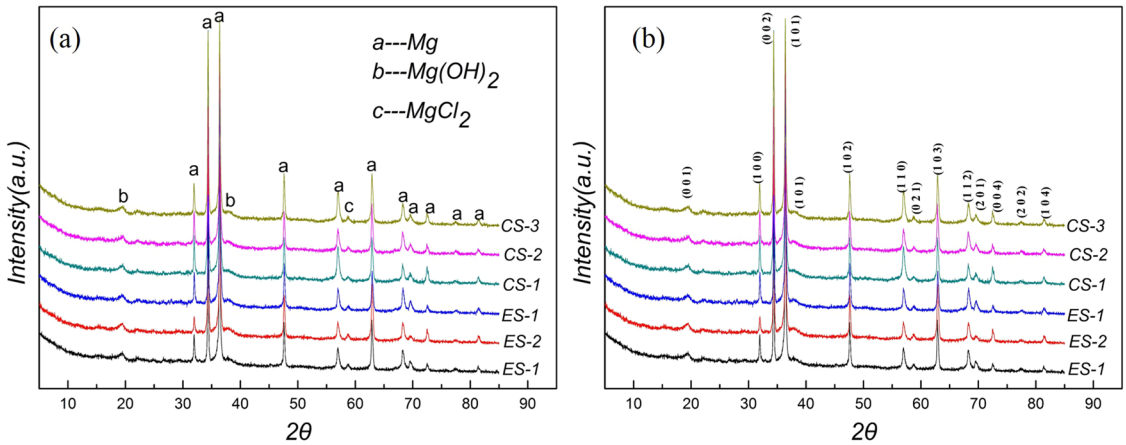

Fig. 4 XRD microanalysis of corrosion products. a Products categories; **b** product crystal surfaces.

dependent on the exposure environment and time[31]. All chloride environments functioned similarly including the marine atmospheric environment because of excess $Mg(OH)_2$ formation either preloaded or as a result of Mg^{2+} release. A thick precipitated $Mg(OH)_2$ film with an inner MgO layer was readily formed in alkaline, chloride environments[32,33]. Oxide thickness was strongly dependent on crystallographic orientation in the chloride containing environment. The corrosion product layers continuously generated inside of the grain, which improved the corrosion potential of α-Mg matrix and prevented electrons transformation. Then the corrosion reaction transformed back to grain boundaries. The EW75 magnesium alloys occurred serious corrosion in cycles in the marine atmospheric environment.

Residual mechanical strength and fracture analysis

The tensile strength, yield strength and elongation of EW75 magnesium alloys measured by universal tensile test machine at the room-temperature. As shown in Fig. 5, for the EW75 extrusion direction samples before exposure corrosion, there were few cleavage steps and secondary cracks in the fracture. Moreover, the fracture was a mixed torn edges and dimple, and local torn edges were connected to with each other. Some dimples were relatively small, showing the characteristics of ductile fracture. However, along the transverse direction samples showed the mixed ductile-brittle fracture, nor was it a typical brittle fracture or a typical ductile fracture[34].

After extrusion deformation and peak-aging, the precipitated phases of EW75 magnesium alloys were distributed uniformly. Both the tensile strength and yield strength had a greatly improvement. As shown in Fig. 6(a), the ultimate tensile strength of the EW75 extrusion direction samples was about 446 MPa, while the yield strength was 385 MPa. Moreover, the elongation of extrusion direction samples even reached up to 12%. The ultimate tensile strength of the EW75 transverse direction samples was about 328 MPa, and the yield strength was 264 MPa, the average value of elongation was about 10%.

Generally, after exposure in the *KEXUE* vessel, corrosion pits and micro-cracks formed in the surface of the magnesium alloys, leading to the decreasing of cross-sectional area. Therefore, the mechanical strength of magnesium alloy declined during the

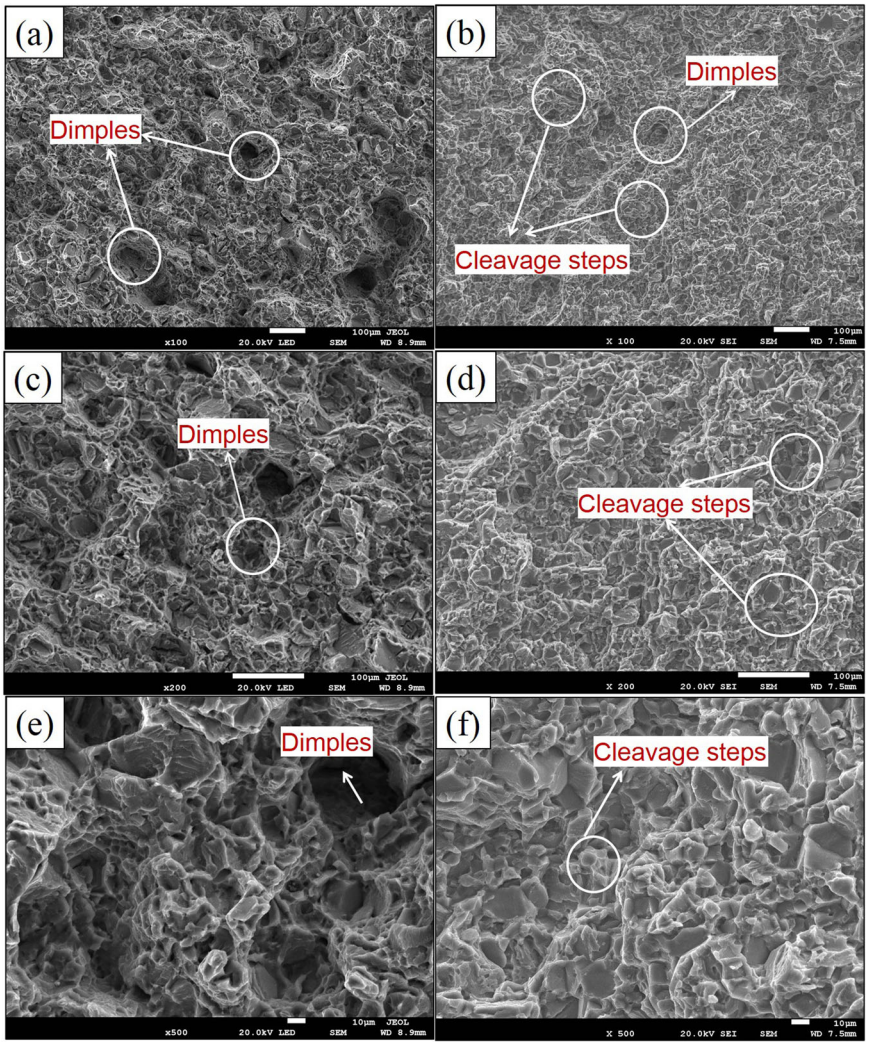

Fig. 5 The fracture morphologies before exposure corrosion. a, **c**, **e** Extrusion direction samples; **b**, **d**, **f** transverse directionsample.

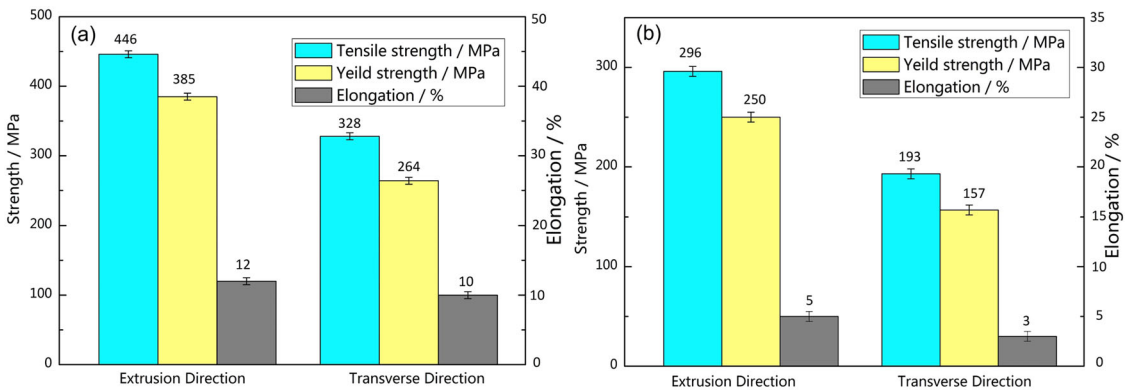

Fig. 6 The mechanical property of the EW75 alloys. Before (**a**) and after (**b**) exposure in KEXUE vessel.

tensile test[35]. As shown in Fig. 6, the average tensile strength of extrusion direction samples decreased from 446 to 296 MPa, indicating that the attenuation ratio was about 33.63%. Moreover, their average yield strength decreased from 385 to 250 MPa, suggesting that the attenuation ratio was about 35.06 %. On the other hand, the tensile strength (328–193 MPa) and yield strength (264–157 MPa) of transverse direction samples decreased about 41.21% and 40.53%, respectively. In conclusion, transverse direction tensile samples showed the more severe corrosion, indicated that the cross-section surface had the lower corrosion resistance of EW75 magnesium alloys.

During the exposure test, corrosion pits occurred on the surface of the samples. With the corrosion reaction processed, the size of corrosion pits gradually increased. The geometrical shape around the pitting pits varied greatly, which resulted a serious stress concentration in this location. Corrosion pits extended to the

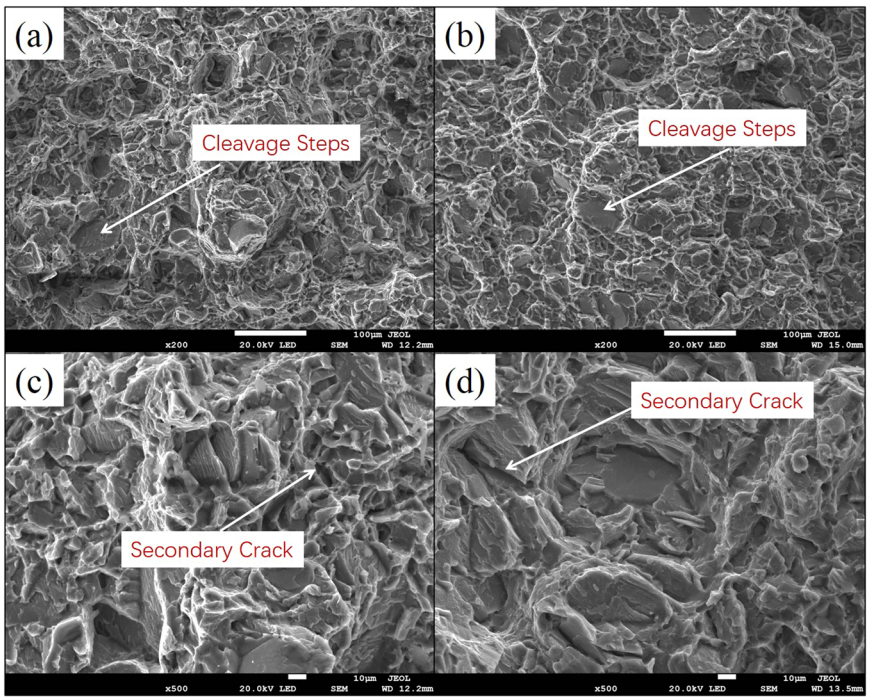

Fig. 7 The fracture morphologies after exposure corrosion. a, **c** Extrusiondirection samples; **b**, **d** transverse direction samples.

depth in the surface of magnesium alloys, resulting in the decreasing of cross-sectional area. This phenomenon caused the increasing of the stress per unit area when the load was applied in the tensile test[36,37].

Figure 7 shows the fracture morphologies of EW75 tensile samples after exposure corrosion for more than 3 months in typical atmospheric environment. It can be seen that there were a lot of cleavage steps and secondary cracks in the fracture, which indicated that the samples occurred the brittle fracture due to the low plasticity. Local areas on the EW75 magnesium alloys surfaces existed amount of corrosion pits, which resulted that the magnesium matrix became loose[38]. In the tensile process of samples, the tolerance of local corrosion areas was lower than the uncorded matrix, which led to the stress concentration in the local corrosion areas. Therefore, the bottom of corrosion pits became the initial location of crack propagation. When the crack propagation size reached up to the critical value, the low stress brittle fracture of EW75 alloys occurred.

The fracture cracks after exposure corrosion by optical microscope was shown in Fig. 8, which displayed that amount of deformation twins existed near the fracture. At the beginning of corrosion reaction, there were only corrosion pits distribution in local positions on the surface of magnesium alloys. With the corrosion reaction processed, the corrosion pits propagated continuously. The crack initiation was controlled by the corrosion. Crystal twins occurred during the tensile deformation of EW75 magnesium alloys. Once the crystal twins formed, the dislocation spreads toward the twin boundaries, which became a potential crack initiation[39]. During the tensile tests, either twin nucleation or crack nucleation in the stress concentration location depended on the energy of twin interface, type of internal defect and experimental conditions[40,41]. The precipitated phases were broken or split off from the α-Mg matrix due to the tensile force, which formed the micro-crack. The surface of EW75 magnesium alloys formed corrosion pits, leading to stress concentration. When the alloys were stretched, stress concentration expanded quickly along the corrosion pits, which was perpendicular to the force direction. Micro-cracks tensile stress continued to grow along the grain boundary or inside the grain, and then become the cracks, which resulted the fracture of EW75 magnesium alloys. This process occurred at the force moment. The plasticity of EW75 alloys reduced rapidly due to the corrosion reaction. This phenomenon proved that the reduction of mechanical property closely related to the early corrosion reaction.

Atmospheric corrosion mechanism in the exposure experiment

The Extrusion Surface along the direction of extrusion deformation, the main grain orientation was (0 0 0 1) base surface. This phenomenon was because that the C axis of close-packed hexagonal (HCP) crystal structure was parallel to the normal direction during the deformation of the EW75 magnesium alloys. In the EW75 alloys, the crystal surfaces were contained (0 0 0 1), (1 0 −1 0) and (2 −1 −1 0). In this study, the distinguishing crystal orientations showed different electrochemical corrosion activity. The larger the volume fraction of (0 0 0 1) crystal surfaces, the corrosion resistance better. Corrosion rate increased accompanied by the reduction of crystal surface intensity of (0 0 0 1) surface, whereas corrosion rate the decreased along with the enlargement of volume fraction of both (1 0 −1 0) and (2 −1 −1 0) crystal surfaces intensity. In the previous studies[42,43], there was a close relationship between corrosion rate and crystal surface energy. The higher of the crystal surface density, the lower the electrochemical corrosion activity, which indicated that the more stable the crystal surface was. In fact, the surface energy of (0 0 0 1) crystal surface is 1.54×10^4 eV/nm^2, whereas these of (1 0 −1 0) and (1 1 −2 0) crystal surfaces was 3.04×10^4 and 2.99×10^4 J/mol, respectively[25,26]. Therefore, the Extrusion Surface samples mainly consisted of (0 0 0 1) crystal surfaces had the better corrosion resistance than the cross-section surface.

During the corrosion reaction, the corrosion product layers formed on the surface could transform a relative steady-state between the EW75 alloy and corrosion environment[37]. During the corrosion process in Marine atmosphere environment, the EW75 alloy rapid corroded in the early stage due to the completed contact with chloride ion, sodium ion, and so on, which resulted a large corrosion rate. The interfacial equilibrium state was EW75

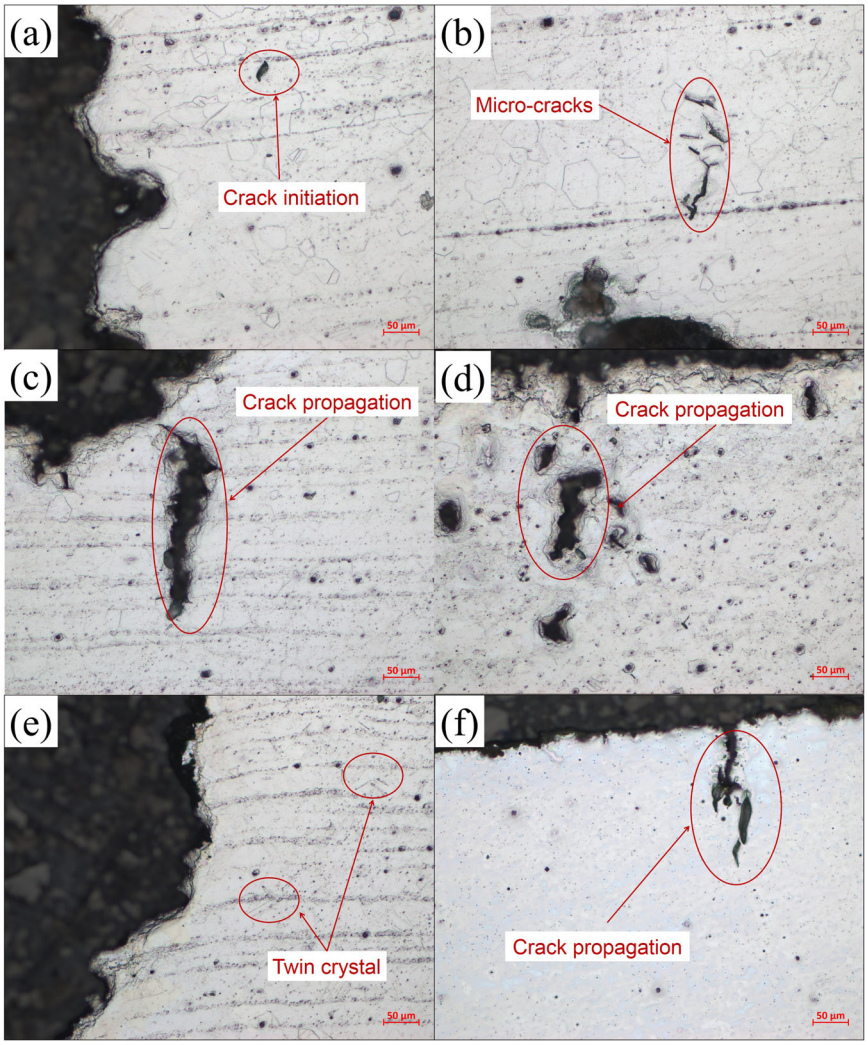

Fig. 8 The fracture cracks after exposure corrosion by optical microscope. a, **c**, **e** Extrusion direction samples; **b**, **d**, **f** transverse directionsamples.

alloy and corrosion environment. During the corrosion medium-term, the insoluble corrosion products formed on the surface of EW75 alloys, which partially inhibited the corrosion reaction. Along with the formation of the corrosion product layer, interface equilibrium changed to double interface, these were "EW75 alloy--corrosion product layer" and "corrosion product layer--corrosion environment". At this time, the corrosion behavior of EW75 alloy affected by the structure and compositions of corrosion product layers, which depended on the relative humidity environment[44]. At the later stage of corrosion, the EW75 alloys surface were covered corrosion product layers. And then the corrosion reaction channel became exactly the pore of corrosion products, resulted that the corrosion process tends maintained to be stable gradually.

As shown in Fig. 9, corrosion environment determined the protection of corrosion products to a large extent. At the initial stage of corrosion, MgO and $MgCl_2$ existed in the corrosion products. With the corrosion reacted gradually, the corrosion products were mainly consisted of $Mg(OH)_2$ and $MgCl_2$. With the erosion of $MgCl_2$ by the splashing seawater and rain water, the protective effect of corrosion products on the matrix was greatly reduced. At this stage, the corrosion product layers were thick and loose. The crystallization of corrosion product layers was coarse and heterogeneous, which were easy to damage, and resulted a serious local corrosion and largest corrosion rate. At the final stage of corrosion, the corrosion products were mainly consisted of $Mg(OH)_2$, which had the compact structure and strong adhesion[45,46]. This corrosion product layers could provide a fine protection for the α-Mg matrix. Meanwhile, the $Mg(OH)_2$ showed a lower conductivity, which resulted that the electron transport efficiency of corrosion reaction was reduced and the dissolution of α-Mg and hydrogen evolution in cathode were impeded, and then the corrosion rate of EW75 alloys decreased. At the final stage of corrosion, the compact corrosion product layers formed and absorbed on the surface of EW75 magnesium alloys, so the type became uniform corrosion.

In the marine atmospheric environment, the temperature and relative humidity were both large during the exposure experiment. Coupled with the effect of wind, the magnesium alloy surface frequently undergoes the dry-wet alternating process. The main environmental factors during the exposure experiment were shown in Table 3. Cl^- was also acted as an important influence factor for corrosion reaction. Cl^- was preferentially adsorbed on the incomplete corrosion production film and breakdown the surface, opening a channel for the further occurrence and development of corrosion. The location of incomplete corrosion production film was preferentially corroded. In addition, the pH of thin liquid film on the surface of EW75 alloys gradually increased with the progress of corrosion. Under the condition of alkaline medium, the protection of corrosion product film enhanced. At

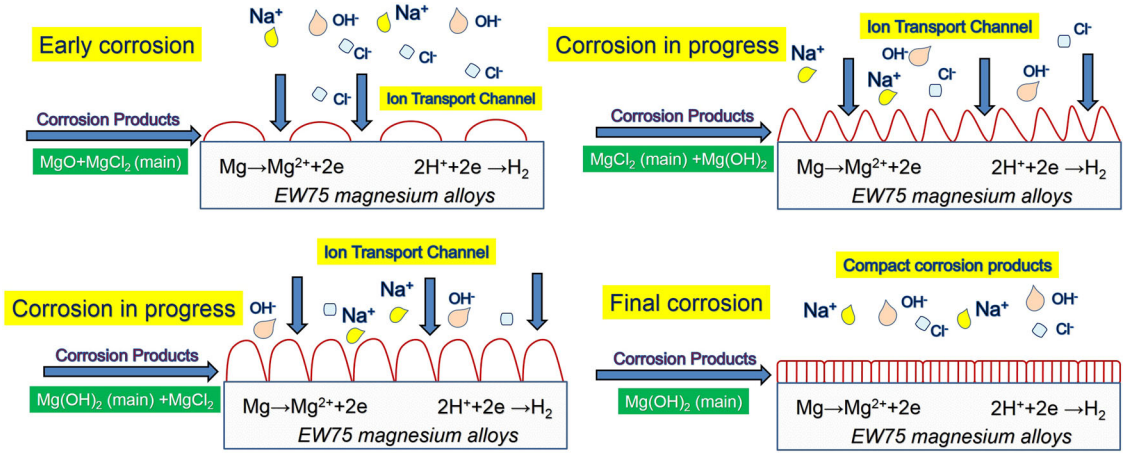

Fig. 9 Schematic related to the corrosion mechanism of EW75 alloys in the exposure tests.

Table 3. The main environmental factors during the exposure experiment.

Exposure period/d	Wind speed/(m/s)	Temperature/(°C)	Relative humidity/(RH)	Atmospheric pressure/(hPa)	Chloride ions mg/(100cm^2 d)
1–30d	6.1	25.8	76.3	1007.9	4.7270
30–60d	6.0	27.9	78.0	1006.6	3.5461
60–90d	3.6	24.0	78.9	1004.1	data loss

this time, Cl^- can only corrode the limited location of incomplete product film. The corrosion of EW75 alloys was characterized by selectivity of Cl^- due to different type of precipitated phases. Under the condition of high relative humidity, the presence of Cl^- promoted the condensation of water vapor, resulted that samples surface formed a thick liquid electrolyte membrane. However, there were no formation of magnesium chloride on the surface of samples. This phenomenon was attributed that magnesium chloride was water-soluble to dissolve in thin liquid film, and the magnesium chloride was washed away by waves. In addition, magnesium hydroxide was more stability than magnesium chloride, and part of the magnesium chloride reacted to produce magnesium hydroxide.

Sample size is also a key factor. Smaller samples tend to have a higher area-normalized corrosion rate than larger samples. The larger the sample size is, the corrosion of the sample is relatively uniform. In order to have a good comparison with our own experimental data, the size of magnesium alloy exposed to corrosion is consistent in previous studies, 5.0 cm × 5.0 cm × 0.3 cm.

The marine atmospheric environment of this western pacific voyage was at the high temperature, high humidity, highly-saline, and intense ultraviolet radiation. During the voyage, the samples were splashed by the nearby ocean waves due to the wind. On the other hand, the location of the exposure corrosion in the *KEXUE* vessel was special. In this area, the surfaces of magnesium alloys were often in a state of alternating wetting and drying due to the periodic wetting of seawater. The oxygen supply was enough during the experiment, coupled with the synergistic action of sunlight, wind and seawater environment, resulting in the most severe corrosion than Qingdao site, Beijing site and South China sea site[19,47].

METHODS

Material preparation and characterization

The Mg-7Gd-5Y-1Nd-0.5Zr (EW75) magnesium alloys were obtained from State Key Laboratory of Nonferrous Material Preparation and Processing, General Research Institute for Nonferrous Metals. The experimental alloys were all smelted with industrial pure magnesium (99.95%), yttrium (99.9%), neodymium (99.9%), Gadolinium (99.9%), and Mg-30Zr intermediate alloys. The ingredients were designed according to Mg-7Gd-5Y-1Nd-0.5Zr. The actual compositions of Mg-7Gd-5Y-1Nd-0.5Zr magnesium alloy, along with the major impurity levels, were detected by inductively coupled plasma atomic emission spectrometry. The chemical compositions of the samples were as follows: Gd, 6.98; Y, 4.72; Nd, 1.14; Zr, 0.41; balance Mg. The ingots were homogenized at (535 °C~24 h) + (250 °C × 5 h), then the multi-directional forging and extrusion deformation were successively carried out. The material used in the experiment was taken from the R/2 circumference of the top of the cast. After homogenization treatment or pre-precipitation heat treatment, the multi-direction forging experiment was carried out in a 1000-ton hydraulic press with a press down rate of 10 mm/s and pass deformation of 5%. Before forging experiment, the sample and cutting board should be placed in the heating furnace for preheating, and the surface of the sample and cutting board should be coated with MoS2 as lubricant during forging. The homogenized samples were forged for six times, and quenched in water immediately after deformation. The diameters of extrusion billet and extrusion specimen were 90 cm and 50 cm, respectively, with a plunger speed of 0.5 mm/s at 573 K. Finally the T5 peak-aging was processed at 220 °C for 6.5 h. These alloys were used as the basic experimental materials in the study.

As shown in Fig. 10, the perpendicular surface to the direction of extrusion deformation was named as the Cross-section Surface, whereas the paralleled surface to the direction of extrusion deformation was the Extrusion Surface. The Cross-section Surface and Extrusion Surface samples were all corroded with 4% nitrate alcohol solution. Then they cleaned and dried with deionized water and anhydrous alcohol[48,49]. The metallographic structures were observed by an optical microscope model (CarlZeiss Axiovet 2000MAT).

The dimension of the sheet samples for the exposure experiments were 5.0 cm × 5.0 cm × 0.3 cm. Firstly, the sheet samples were polished by SiC abrasive paper (240~5000#) and polishing machine (PG-2), and then cleaned and dried successively with deionized water and ethanol. Both Cross-section Surface and Extrusion Surface samples had three parallel sheet samples to ensure the accuracy of experiment results. The weight of different samples was tested via the analytical balance. Original weight (W_0), original thickness and surface area (S) were all recorded before the exposure corrosion. Exposure corrosion rack was used to attach the samples.

The extrusion direction and transverse direction tensile samples were selected in accordance with the direction shown in Fig. 1. The dimension of tensile samples was processed according to GB/T228-2002.The thread

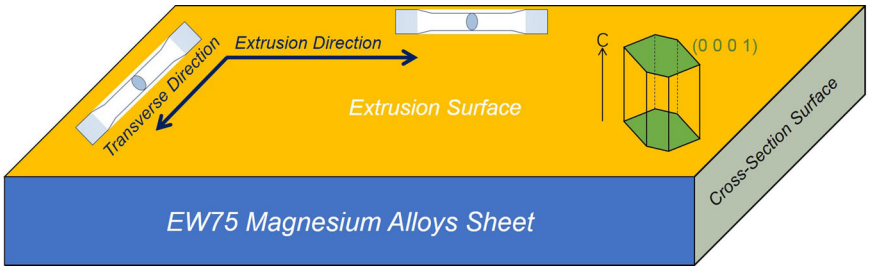

Fig. 10 The schematic diagram of sheet samples and tensile samples of EW75 alloys.

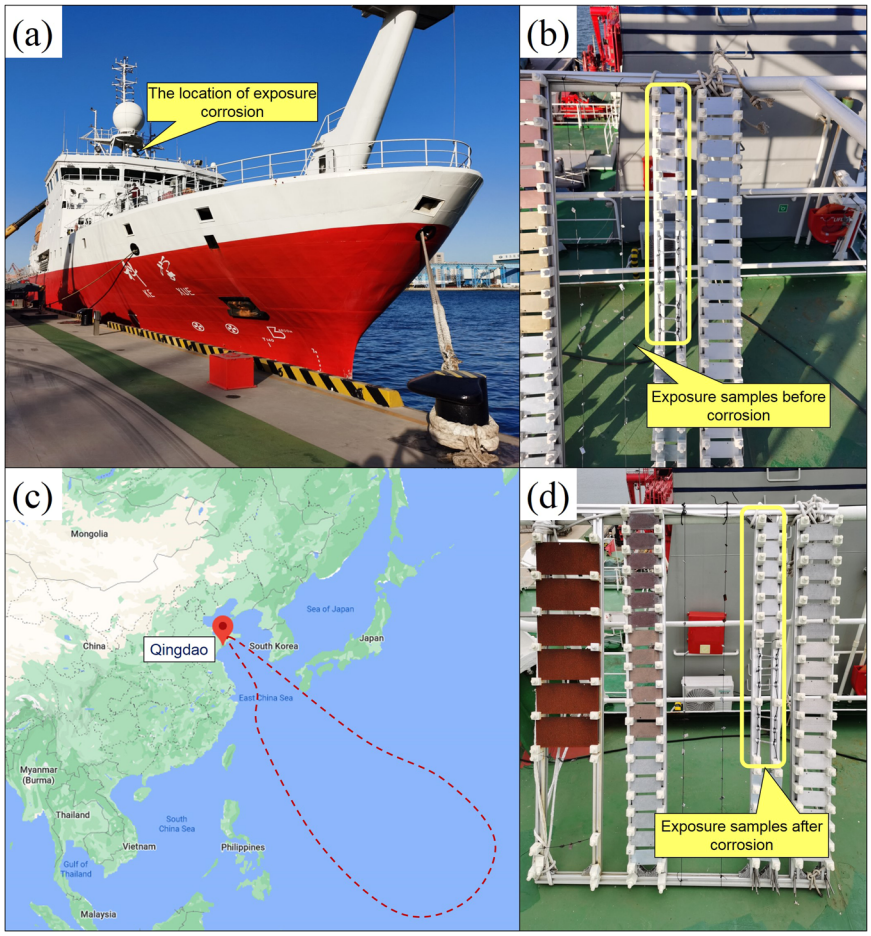

Fig. 11 The photographs of corrosion experiments in the *RV KEXUE*. **a** *RV KEXUE*, **b** samples before exposure corrosion, **c** ocean voyage, **d** samples after exposure corrosion.

locations of tensile samples were protected with polytetrafluoroethylene belts (around 20–25 laps) to prevent the thread locations from corrosion.

The mechanical properties of tensile samples before and after exposure corrosion experiments were tested according to GB228-87 standard. After exposure corrosion experiments, amount of corrosion products was existed on the samples surface. The mechanical properties were tested at room temperature by AG-250KNIS universal tensile machine. The tensile rate was at 2 mm/min.

To conduct microstructural analysis, samples were prepared by polishing and etching in a weak solution of nitric acid and alcohol. The ethanol was used to clean the surfaces of samples. The microstructure, precipitated phases and surface morphology after corrosion were all measured by SEM (JSF-6700F), and the texture and grain size of the EW75 magnesium alloy were determined by the electron backscatter diffraction (EBSD) technique. The characteristic peaks of EW75 alloys were tested by XRD (D/Max 2550), whereas the test step was 4°/min.

Exposure tests in the *RV KEXUE*

The exposure corrosion experiments of EW75 magnesium alloys were carried out in the *RV KEXUE* during the ocean voyage from May 12th 2020 to August 17th 2020 (Fig. 11a, b). The *RV KEXUE* is one of the national major science and technology infrastructures to undertake multi-disciplinary ocean research. The ship was designed by Marine Design & Research Institute of China, and built by Wuchang Shipbuilding Industry Co., Ltd, which was delivered in 2012 and is operated by the Institute of Oceanology, Chinese Academy of Sciences.

During this exposure experiments, the *RV KEXUE* sailed from Qingdao, and the voyage was around the western pacific, finally the vessel returned to Qingdao (Fig. 11c). The marine atmospheric environment of this western pacific voyage was at the high temperature, high humidity, highly-saline, and intense ultraviolet radiation. During the voyage, the samples of EW75 magnesium alloys often were splashed by the nearby ocean waves due to the strong wind. The main positive ions in the atmospheric environment

were contained Na^+, Mg^{2+}, Ca^{2+} and K^+, whereas negative ions were main contained Br^- and Cl^-. The samples on the test stand after the *RV KEXUE* back to Qingdao were shown in Fig. 11d.

After the exposure corrosion tests, corrosion depths on the surfaces of different samples were measured by the thickness gauge (Instrument type: GTS8102). The thickness gauge needs to be calibrated using the standard EW75 alloys without corrosion. Each corrosion samples tested five different locations (four corners and center of the square surface) on the surfaces of magnesium alloys. All the testing surfaces selected the sides facing the forward of the *RV KEXUE*, which corroded more seriously than the reverse sides because of the rain and ultraviolet radiation.

The EW75 alloys immersed into the chromic acid, and then heated the solution to a boiling state to remove the corrosion products. Next, deionized water and ethyl alcohol were used to flush the surfaces. Finally, analytical balance was employed to measure the final weight (W_1) of the drying samples. The weight loss after exposure corrosion obtained from the difference between W_0 and W_1[50,51].

DATA AVAILABILITY

All data included in this study are available upon request by contact with the corresponding author.

Received: 28 December 2021; Accepted: 12 March 2022;
Published online: 12 April 2022

REFERENCES

1. Rokhlin, L. L. *Mg Alloys Containing Rare Earth Metals: Structure and Properties* (*Crc Press*, 2003).
2. You, S., Huang, Y., Kainer, K. U. & Hort, N. Recent research and developments on wrought magnesium alloys. *J. Magnes. Alloy* **5**, 239–253 (2017).
3. Jiang, Q., Lv, X., Lu, D., Zhang, J. & Hou, B. The corrosion behavior and mechanical property of the Mg-7Y-xNd ternary alloys. *J. Magnes. Alloy* **6**, 346–355 (2018).
4. Takenaka, T., Ono, T., Narazaki, Y., Naka, Y. & Kawakami, M. Improvement of corrosion resistance of magnesium metal by rare earth elements. *Electrochim. Acta* **53**, 117–121 (2007).
5. Jiang, Q., Yang, L. & Hou, B. The effect of deep cryogenic treatment on the corrosion behavior of Mg-7Y-1.5Nd magnesium alloy. *Metals* **7**, 427 (2017).
6. Birbilis, N., Easton, M. A., Sudholz, A. D., Zhu, S. M. & Gibson, M. A. On the corrosion of binary magnesium-rare earth alloys. *Corros. Sci.* **51**, 683–689 (2009).
7. Jiang, Q. et al. Corrosion behaviors for peak-aged Mg-7Gd-5Y-1Nd-0.5Zr alloys with oxide films. *Rare. Met.* **35**, 758–762 (2016).
8. Xia, X., Zhang, K., Li, X., Ma, M. & Li, Y. Microstructure and texture of coarse-grained Mg-Gd-Y-Nd-Zr alloy after hot compression. *Mater. Des.* **44**, 521–527 (2013).
9. Li, T. et al. Dynamic precipitation during multi-axial forging of an Mg-7Gd-5Y-1Nd-0.5Zr alloy. *J. Magnes. Alloy* **1**, 47–53 (2013).
10. Wu, D., Chen, R. S. & Ke, W. Microstructure and mechanical properties of a sand-cast Mg-Nd-Zn alloy. *Mater. Des.* **58**, 324–331 (2014).
11. Aghion, E., Gueta, Y., Moscovitch, N. & Bronfin, B. Effect of yttrium additions on the properties of grain-refined Mg-3%Nd alloy. *J. Mater. Sci.* **43**, 4870–4875 (2008).
12. Mirza, F. A., Chen, D. L., Li, D. J. & Zeng, X. Q. Low cycle fatigue of an extruded Mg-3Nd-0.2Zn-0.5Zr magnesium alloy. *Mater. Des.* **64**, 63–73 (2014).
13. Liao, J., Hotta, M., Motoda, S. I. & Shinohara, T. Atmospheric corrosion of two field-exposed AZ31B magnesium alloys with different grain size. *Corros. Sci.* **71**, 53–61 (2013).
14. Liao, J. & Hotta, M. Corrosion products of field-exposed Mg-Al series magnesium alloys. *Corros. Sci.* **112**, 276–288 (2016).
15. Jönsson, M., Persson, D. & Leygraf, C. Atmospheric corrosion of field-exposed magnesium alloy AZ91D. *Corros. Sci.* **50**, 1406–1413 (2008).
16. Cui, Z., Li, X., Xiao, K. & Dong, C. Atmospheric corrosion of field-exposed AZ31 magnesium in a tropical marine environment. *Corros. Sci.* **76**, 243–256 (2013).
17. Cui, Z. Y. et al. Pitting corrosion behaviour of AZ31 magnesium in tropical marine atmosphere. *Corros. Eng. Sci. Technol.* **49**, 363–371 (2014).
18. Liu, H. et al. Review of the atmospheric corrosion of magnesium alloys. *J. Mater. Sci. Technol.* **35**, 2003–2016 (2019).
19. Jiang, Q. et al. The corrosion behavior of Mg-Nd binary alloys in the harsh marine environment. *J. Magnes. Alloy* **9**, 292–304 (2021).
20. Jiang, Q. et al. Atmospheric corrosion of Mg-rare earth alloy in typical inland and marine environments. *Corros. Eng. Sci. Technol.* **49**, 651–655 (2014).
21. Li, T. et al. Characterisation of precipitates in a Mg-7Gd-5Y-1Nd-0.5Zr alloy aged to peak-ageing plateau. *J. Alloy. Compd.* **574**, 174–180 (2013).
22. Li, T. et al. Characterization of β precipitate phase in Mg-7Gd-5Y-1Nd-0.5Zr alloy. *J. Rare. Earth.* **31**, 410–414 (2013).
23. Li, T. et al. Morphology and crystallography of β precipitate phase in Mg-Gd-Y-Nd-Zr alloy. *T. Nonferr. Metal. Soc.* **22**, 2877–2882 (2012).
24. Wang, B. J., Xu, D. K., Dong, J. H. & Ke, W. Effect of the crystallographic orientation and twinning on the corrosion resistance of an as-extruded Mg-3Al-1Zn (wt.%) bar. *Scr. Mater.* **88**, 5–8 (2014).
25. Song, G. L., Mishra, R. & Xu, Z. Crystallographic orientation and electrochemical activity of AZ31 Mg alloy. *Electrochem. Commun.* **12**, 1009–1012 (2010).
26. Xin, R., Li, B., Li, L. & Liu, Q. Influence of texture on corrosion rate of AZ31 Mg alloy in 3.5 wt.% NaCl. *Mater. Des.* **32**, 4548–4552 (2011).
27. Song, G. L. & Xu, Z. Crystal orientation and electrochemical corrosion of polycrystalline Mg. *Corros. Sci.* **63**, 100–112 (2012).
28. Yang, L. J. et al. Atmospheric corrosion of field-exposed AZ91D Mg alloys in a polluted environment. *Corros. Sci.* **52**, 2188–2196 (2010).
29. Sun, S., Zheng, Q., Li, D., Hu, S. & Wen, J. Exfoliation corrosion of extruded 2024-T4 in the coastal environments in China. *Corros. Sci.* **53**, 2527–2538 (2011).
30. Cao, F. et al. Corrosion of ultra-high-purity Mg in 3.5% NaCl solution saturated with Mg $(OH)_2$. *Corros. Sci.* **75**, 78–99 (2013).
31. Song, G. L. & Atrens, A. Corrosion mechanisms of magnesium alloys. *Adv. Eng. Mater.* **1**, 11–33 (1999).
32. Winzer, N. et al. A critical review of the stress corrosion cracking (SCC) of magnesium alloys. *Adv. Eng. Mater.* **7**, 659–693 (2005).
33. Merson, E., Poluyanov, V., Myagkikh, P., Merson, D. & Vinogradov, A. Inhibiting stress corrosion cracking by removing corrosion products from the Mg-Zn-Zr alloy pre-exposed to corrosion solutions. *Acta Mater.* **205**, 116570 (2021).
34. Wang, L., Liang, J., Li, H., Cheng, L. & Cui, Z. Quantitative study of the corrosion evolution and stress corrosion cracking of high strength aluminum alloys in solution and thin electrolyte layer containing Cl. *Corros. Sci.* **178**, 109076 (2021).
35. Bland, L. G., Scully, L. C. & Scully, J. R. Assessing the corrosion of multi-phase Mg-Al alloys with high al content by electrochemical impedance, mass loss, hydrogen collection, and inductively coupled plasma optical emission spectrometry solution analysis. *Corrosion* **73**, 526–543 (2017).
36. Bland, L. G., Fitz-Gerald, J. M. & Scully, J. R. Metallurgical and electrochemical characterization of the corrosion of AZ31B-H24 tungsten inert gas weld: isolated weld zones. *Corrosion* **72**, 1116–1132 (2016).
37. Bland, L. G., Rincon Troconis, B. C., Santucci, R. J. Jr., Fitz-Gerald, J. M. & Scully, J. R. Metallurgical and electrochemical characterization of the corrosion of a Mg-Al-Zn Alloy AZ31B-H24 tungsten inert gas weld: galvanic corrosion between weld zones. *Corrosion* **72**, 1226–1242 (2016).
38. Zhang, X., Dai, J., Zhang, R., Ba, Z. & Birbilis, N. Corrosion behavior of Mg-3Gd-1Zn-0.4Zr alloy with and without stacking faults. *J. Magnes. Alloy* **7**, 240–248 (2019).
39. Song, G. L. & Xu, Z. The surface, microstructure and corrosion of magnesium alloy AZ31 sheet. *Electrochim. Acta* **55**, 4148–4161 (2010).
40. Liu, X., Shan, D., Song, Y. & Han, E. H. Influence of yttrium element on the corrosion behaviors of Mg-Y binary magnesium alloy. *J. Magnes. Alloy* **5**, 26–34 (2017).
41. Atrens, A., Winzer, N., Song, G., Dietzel, W. & Blawert, C. Stress corrosion cracking and hydrogen diffusion in magnesium. *Adv. Eng. Mater.* **8**, 749–751 (2006).
42. Fu, Y., Li, J., Luo, H., Du, C. & Li, X. Recent advances on environmental corrosion behavior and mechanism of high-entropy alloys. *J. Mater. Sci. Technol.* **80**, 217–233 (2021).
43. Sun, S., Zheng, Q., Li, D. & Wen, J. Long-term atmospheric corrosion behaviour of aluminium alloys 2024 and 7075 in urban, coastal and industrial environments. *Corros. Sci.* **51**, 719–727 (2009).
44. Sudholz, A. D. et al. Electrochemical behaviour and corrosion of Mg-Y alloys. *Corros. Sci.* **53**, 2277–2282 (2011).
45. Bland, L. G., Gusieva, K. & Scully, J. R. Effect of crystallographic orientation on the corrosion of magnesium: comparison of film forming and bare crystal facets using electrochemical impedance and Raman spectroscopy. *Electrochim. Acta* **227**, 136–151 (2017).
46. Jiang, Q. et al. Anisotropy of the crystallographic orientation and corrosion performance of high-strength AZ80 Mg alloy. *J. Magnes. Alloy* **3**, 309–314 (2015).
47. Li, Y. G., Wei, Y. H., Hou, L. F. & Han, P. J. Atmospheric corrosion of AM60 Mg alloys in an industrial city environment. *Corros. Sci.* **69**, 67–76 (2013).
48. Williams, G., Gusieva, K. & Birbilis, N. Localized corrosion of binary Mg-Nd alloys in chloride-containing electrolyte using a scanning vibrating electrode technique. *Corrosion* **68**, 489–498 (2012).
49. Zucchi, F., Grassi, V., Frignani, A., Monticelli, C. & Trabanelli, G. Electrochemical behaviour of a magnesium alloy containing rare earth elements. *J. Appl. Electrochem.* **36**, 195–204 (2006).
50. Wang, P., Zhang, D., Qiu, R., Wu, J. & Wan, Y. Super-hydrophobic film prepared on zinc and its effect on corrosion in simulated marine atmosphere. *Corros. Sci.* **69**, 23–30 (2013).
51. Chang, J. et al. Investigation of the corrosion for Mg-xGd-3Y-0.4Zr (x = 6, 8, 10, 12 wt%) alloys in a peak-aged condition. *Corros. Sci.* **50**, 166–177 (2008).

ACKNOWLEDGEMENTS

The authors gratefully acknowledge National Natural Science Foundation of China for Exploring Key Scientific Instrument (No. 41827805), the Open Funds of the State Key Laboratory of Rare Earth Resource Utilization (No. RERU2021017) and Hainan Province Science and Technology Special Fund (ZDYF2021GXJS210) for providing support. Acknowledgement for the Data Support from Institute of Oceanology of the Chinese Academy of Sciences Marine Science Data Center and *RV KEXUE*.

AUTHOR CONTRIBUTIONS

Q.J. and L.C. conceived and designed the study and experiment plan. D.L. performed the experiments. Q.J. and N.L. analyzed the data. B.H. verified the experimental results. Q.J. wrote the paper. D.L., N.L., and B.H. reviewed and edited the paper. L.Y. collected the environmental data. All authors read and approved the paper.

COMPETING INTERESTS

The authors declare no competing interests.

ADDITIONAL INFORMATION

Correspondence and requests for materials should be addressed to Quantong Jiang.

Reprints and permission information is available at http://www.nature.com/reprints

Publisher's note Springer Nature remains neutral with regard to jurisdictional claims in published maps and institutional affiliations.